Fabrication and electrical characterization of a silicon Schottky device based on organic material

2009 Phys. Scr. 79 035802

(http://iopscience.iop.org/1402-4896/79/3/035802)

IOP Publishing Physica Scripta
Phys. Scr. **79** (2009) 035802 (6pp) doi:10.1088/0031-8949/79/03/035802

Fabrication and electrical characterization of a silicon Schottky device based on organic material

Ş Aydoğan, Ö Güllü and A Türüt

Faculty of Science, Department of Physics, Atatürk University, Erzurum, Turkey

E-mail: omergullu@gmail.com

Received 23 June 2008
Accepted for publication 13 January 2009
Published 3 March 2009
Online at stacks.iop.org/PhysScr/79/035802

Abstract
An Al/methyl violet (MV)/n-Si/AuSb Schottky structure was fabricated and its current–voltage (*I–V*), capacitance–voltage (*C–V*) and capacitance–frequency (*C–f*) characteristics were investigated at room temperature. A modified Norde's function combined with conventional forward *I–V* method was used to extract the parameters including barrier height (BH) and series resistance. The BH and series resistance obtained from Norde's function have been compared with those from Cheung functions, and it was seen that there is good agreement between the BH values from both methods. It was also seen that the values of capacitance are almost independent of frequency up to a certain value of frequency, whereas at high frequencies the capacitance decreased. The higher values of capacitance at low frequencies were attributed to the excess capacitance resulting from the interface states in equilibrium with the n-Si that can follow the alternating current (ac) signal.

PACS numbers: 85.30.Hi, 85.30.Kk, 73.30.+y

1. Introduction

Organic electronics has attracted considerable interest, because organic materials have several distinguishing features: process ability, cost effectiveness, high damage threshold, large nonlinearity and the ease with which large crystals of high optical quality can be grown and fabricated into desired shapes [1]. Apart from the electronic properties of the organic films, the properties of their associated interfaces are important factors for thin-film organic device function: the interface to the substrate not only mediates the organic film growth and its electronic properties, but also determines the injection efficiency of the contact [2]. Semiconducting organic materials can be used in different condensed matter physics applications, such as organic light-emitting diodes, organic field effect transistors, Schottky diodes, photovoltaic (PV) and solar cells, organic spintronics and so on. Furthermore, more recently, electronic systems are moving to the ultimate scale of molecular entities, as demonstrated by the growing interest in understanding transport through organic molecules bridging two metal contacts [3–5]. Methyl violet (MV) with molecular formula $C_{25}H_{30}ClN_3$ used in this work is a typical aromatic azo compound. It is an organic dye molecule used extensively as an acid–base indicator due to its radical color change with varying pH. Its color originates from absorbance in the visible region of the spectrum due to the delocalization of electrons in the benzene and azo groups forming a conjugated system. The molecular structure of the MV is given in figure 1(a). Recently the structure of azo dyes has attracted considerable attention due to their wide applicability in the light-induced photo isomerization process and their potential usage for reversible optical data storage [6].

In a Schottky diode some parameters, such as ideality factor, barrier height (BH) and series resistance, affect the performance of the device. These parameters give useful information about the nature of the diode. In most metal–semiconductor (MS) contacts, there is an unavoidable native thin insulating layer of oxide on the surface of the semiconductor. This layer converts the MS structure into a metal/insulator/semiconductor (MIS) device. Because Schottky BHs (SBHs) of MS contacts can be manipulated by insertion of a dipole layer between the semiconductor and the organic film. To date, many attempts have been made to realize a modification and the continuous control of the BH using an organic semiconducting layer, an insulating

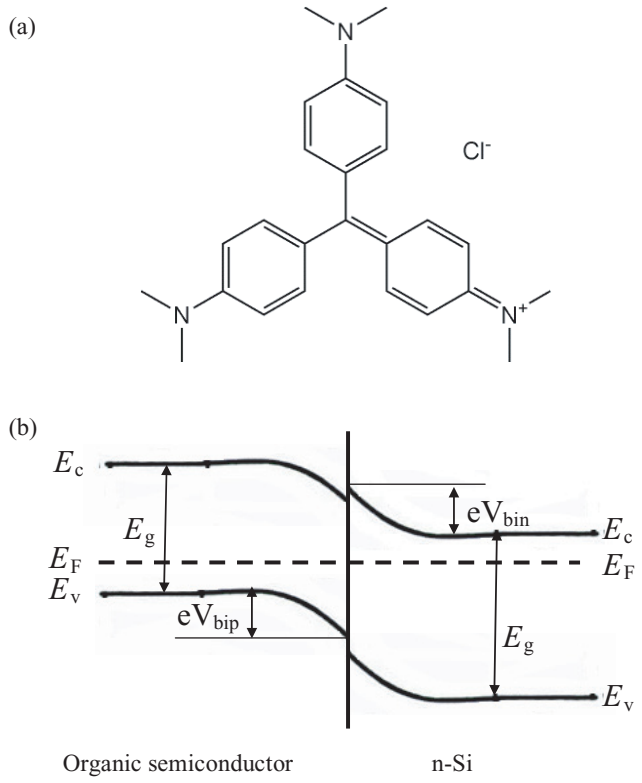

Figure 1. (a) Chemical structure of MV. (b) Energy band diagram of the organic–inorganic semiconductor device at thermal equilibrium.

layer and/or a chemical passivation procedure at certain metal/inorganic semiconductor interfaces, or to determine characteristic parameters of organic film [6–16]. Campbell *et al* [7] have used an organic thin film to introduce a controlled dipole layer at the semiconductor/organic interface and thus change the effective SBH. They [7] reported that the effective Schottky barrier could be either increased or decreased by using an organic thin layer on an inorganic semiconductor.

Our aim is to fabricate an Al/MV/n-Si/AuSb and to study the suitability and possibility of organic-on-inorganic semiconductor contacts for use in barrier modification of the Si MS diode. For this purpose, we investigate some junction parameters of the structure by electrical measurements such as current–voltage (*I–V*) and capacitance–voltage–frequency (*C–V–f*).

2. Experimental procedure

An n-type Si semiconductor wafer with (100) orientation, 400 μm thickness and 1–10 Ω cm resistivity was used in this study. The wafer was chemically cleaned using the RCA cleaning procedure (i.e. 10 min boiling in $NH_3 + H_2O_2 + 6H_2O$ followed by 10 min $HCl + H_2O_2 + 6H_2O$ at 60 °C). Ohmic back contact was made by evaporating Au–Sb alloy on the back of n-Si substrate, and then it was annealed at 420 °C for 3 min in N_2 atmosphere. Native oxide on the front surface of the substrate was removed in $HF + 10H_2O$ solution. Finally, it was rinsed in de-ionized water for 30 s and was dried in N_2 atmosphere before forming an organic layer on the n-type Si substrate. MV organic film was directly formed by adding 6 μl of MV solution (0.2 wt.% in methanol) on the front surface of the n-Si wafer, and dried by itself in N_2 atmosphere for 1 h. The thickness of the MV film on n-Si was calculated as 55 nm from high-frequency *C–V* measurements at 1000 kHz in the accumulation state. To perform electrical measurements, Al top contact metal was evaporated on the MV at 10^{-5} Torr (diode area $A = 7.85 \times 10^{-3}$ cm^2). Figure 1(b) shows the energy-band diagram for the organic/n-Si structure at the thermal equilibrium condition [17]. In figure 1(b), V_{bin} is the built-in potential for electrons in n-Si, and V_{bip} is the built-in potential for holes in the organic semiconductor. E_g is the forbidden band gap energy, E_F the Fermi level, E_v the energy level of the top of the valance band and E_C the energy level of the bottom of the conduction band for semiconductors. *I–V* and *C–V–f* measurements of the Al/MV/n-Si/AuSb structure were performed with a KEITLEY 487 Picoammeter/Voltage Source and an HP 4192A (50 Hz–13 MHz) LF IMPEDENCE ANALYZER, respectively.

3. Results and discussion

A Schottky contact current flow can be described by the well-known thermionic emission (TE) theory given as follows [17]:

$$I = I_0 \left[\exp\left(\frac{qV}{nkT}\right) - 1 \right], \tag{1}$$

where

$$I_0 = AA^*T^2 \exp\left(-\frac{q\Phi_b}{kT}\right) \tag{2}$$

is the saturation current. Φ_b is the effective BH at zero bias, A^* the Richardson constant and equal to 112 A cm^{-2} K^2 for n-type Si, q the electron charge, V the applied voltage, A the diode area, k the Boltzmann constant, T the temperature in kelvin and n the ideality factor. n is determined from the slope of the linear region of the forward bias ln *I–V* characteristic through the relation

$$n = \frac{q}{kT}\frac{dV}{d(\ln I)}. \tag{3}$$

n equals one for an ideal diode. However, n usually has a value greater than unity. High values of n can be attributed to the presence of the interfacial thin native oxide layer, a wide distribution of low-SBH patches (or barrier inhomogeneities) and the bias voltage dependence of the SBH [17, 18]. Φ_b is the zero-bias BH, which can be obtained from the following equation:

$$\Phi_b = kT/q \ \ln\left(AA^*T^2/I_0\right). \tag{4}$$

Figure 2 shows the forward bias *I–V* characteristics of the Al/MV/n-Si/AuSb structure. The values of the n and Φ_b obtained from *I–V* characteristics using equations (3) and (4) are 3.38 and 0.78 eV, respectively. The high value in the ideality factor is caused possibly by organic interlayer plus native oxide film between the top metal and the inorganic semiconductor. According to Cakar *et al* [15], equation (1) can be fitted to experimental *I–V* data of this device by using n, Φ_b, series resistance (R_s) and shunt resistance (R_p). In this way, continuous curves in figure 2 for forward and reverse

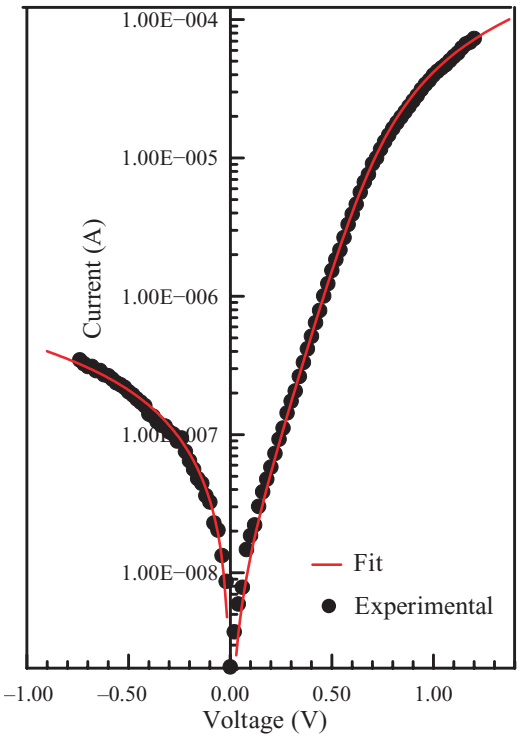

Figure 2. Experimental *I–V* characteristic of the Al/MV/n-Si/AuSb structure.

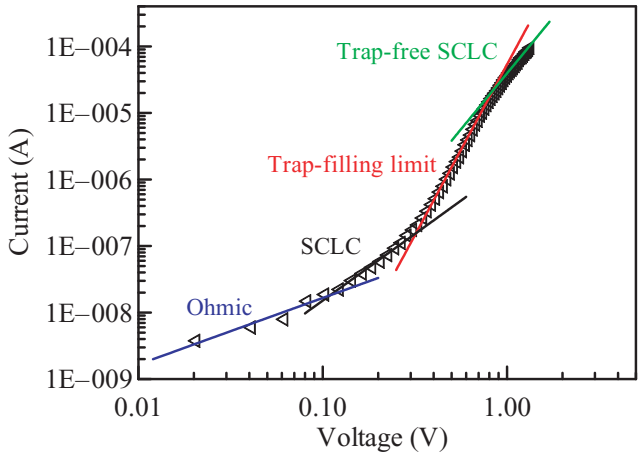

Figure 3. Log *I*–log *V* plot of the Al/MV/n-Si/AuSb structure at forward bias.

bias regions were plotted with the fitting parameter values of $R_p = 100\,\Omega$, $R_s = 5\,k\Omega$, $\Phi_b = 0.78\,eV$ and $n = 3.48$, and $R_p = 2.1 \times 106\,\Omega$, $R_s = 3.1 \times 10^8\,\Omega$, $\Phi_b = 0.87\,eV$ and $n = 4$, respectively. A downward concave curvature in the forward bias *I–V* plot for sufficiently large voltages is seen in figure 2. In the organic/inorganic structures it is well known that the so-called 'downward concave curvature' of current for forward values of bias may be assigned to the occurrence of the space-charge-limited current (SCLC) conduction effect. Therefore, a forward bias log*I*–log*V* plot of the device was drawn as given in figure 3. Under forward bias, our organic-based Schottky diode reveals four distinct regimes as shown in figure 3: Ohmic, SCLC, trap filling limit (TFL) and trap-free SCLC regimes [19, 20].

Our device with the Al cathode shows that the carrier injection limitation is located at the organic/cathode interface

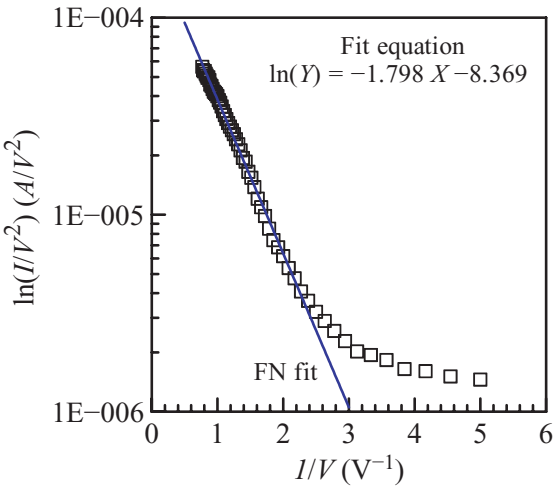

Figure 4. FN plot of the Al/MV/n-Si/AuSb structure at forward bias.

and the Fowler–Nordheim (FN) mechanism is qualitatively consistent with experimental data at high voltages. Therefore, a mechanism different from termionic emission seems to become dominant to limit the current at high voltages. Figure 4 shows the *I–V* data in the $\ln(I/V^2)$ versus I/V plot to see if it fits with the FN tunneling formula [21]

$$I \alpha F^2 e^{-\kappa/F}, \tag{5}$$

where $F = V/d$ is the electric field strength and κ is a parameter that depends on barrier shape. Assuming the injected charge is tunneling through a triangular barrier, the constant κ in equation (5) is given by

$$\kappa = 8\pi(2m^*)^{1/2}\varphi^{3/2}/3qh, \tag{6}$$

where φ is the Schottky energy barrier, m^* the effective mass of the charge carriers, q the magnitude of the electronic charge and h the Planck's constant [21]. In the process of injection, if the device obeys the FN tunneling mechanism, the log of current will exhibit a linear relationship with the reciprocal value of the field. It can be seen that the *I–V* data in figure 4 fit very well with the FN tunneling formula in a wide range of the current at high voltages for the device. From the slope of the straight line, the injection BH for carriers is estimated. The BH was calculated as 0.76 eV for the device. Our result is in good agreement with that obtained from equation (4).

As can be seen, the Φ_b value of 0.78 eV that we have obtained for the Al/MV/n-S structure due to the MV organic layer is remarkably higher than those achieved with conventional MS contacts such as Al/n-Si Schottky diodes, where $\Phi_b = 0.50\,eV$ [17]. Furthermore, the Φ_b value of 0.78 eV that we found for the Al/MV/n-Si structure is higher than the value of 0.71 eV given for PPy/n-Si device in [22]. The case may be ascribed to the MV interlayer modifying the effective BH by influencing the space-charge region of the inorganic silicon substrate [16]. Thereby, it is known that the MV film forms a physical barrier between the metal and the Si inorganic substrate, preventing the metal from directly contacting the Si surface. The MV organic layer appears to cause significant modification of the interface states even though the organic–inorganic interface becomes abrupt and unreactive [15, 16, 23–26]. Thus, the

change in BH can qualitatively be explained by an interface dipole induced by organic layer passivation [23–26]. Kampen *et al* [24] have observed by photoemission spectroscopy investigations that S passivation reduces surface band bending on n-type-doped GaAs; on the other hand, band bending on the surfaces of p-type-doped GaAs increases. Similarly, Zahn *et al* [26] have indicated that the initial increase or decrease in effective BH for the organic interlayer is correlated with the energy level alignment of the lowest unoccupied molecular orbital (LUMO) with respect to the conduction band minimum (CBM) of the inorganic semiconductor at the organic–inorganic semiconductor interface.

This structure shows organic-on-inorganic semiconductor heterojunction (OI-HJ) behavior and exhibits a rectification whereby the *I–V* characteristics are limited by the properties of the inorganic semiconductor substrate and the magnitude of the energy barrier at the hetero-interface at the low applied voltage. That is, the OI-HJ structures behave like an MS Schottky contact at the low current or applied voltage. The case shows that the TE over the MV/n-Si contact barrier may be important at low current densities [24–26]. At high current densities, space-charge injection (the SCLC) across the MV layer is dominant and is limited by charged states at the contact metal/MV interface [27, 28]. It is known that a mean BH value of 0.78 eV is the contact potential barrier that exists at the interface between the organic and inorganic layers, i.e. at the MV/n-Si interface. The heterojunction BH Φ_b controls the injection of charge from the metal/organic contact into the inorganic semiconductor substrate n-Si. The presence of the BH Φ_b results in the rectification of current by the OI-HJ. In reverse bias (i.e. where the AuSb back ohmic contact is at a positive potential relative to the Al top contact on the MV), the carriers must overcome the barrier potential. Under forward bias, the carriers are injected from the Si substrate into the organic thin film, which ultimately limits the current due to the small mobilities [29]. Furthermore, there is also an interface dipole layer or contact potential barrier at the interface between the Al and MV layers that would affect the contact potential barrier that exists at the interface between Al/MV [15, 30]. This layer contributes to the potential drop (dipole) across the metal/organic interface and a modification of the metal work function due to the adsorption of the organic molecules and a potential change in the organic semiconductor [15, 30].

It is well known that the downward concave curvature of the forward bias *I–V* plots at sufficiently large voltages is caused by the presence of the effect of series resistance, apart from interface states, which are in equilibrium with the semiconductor [31]. The R_s values were calculated using a method developed by Cheung and Cheung [32, 33]. According to Cheung and Cheung [33], the forward bias *I–V* characteristics due to the TE of a Schottky diode with series resistance can be expressed as

$$I = I_0 \exp\left[\frac{q\,(V - IR_s)}{nkT}\right], \tag{7}$$

where the IR_s term is the voltage drop across the series resistance of the device. The values of the series resistance can be determined from the following functions using

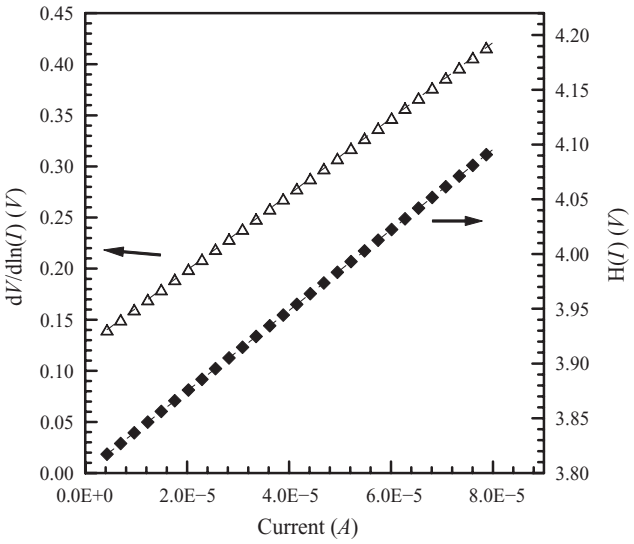

Figure 5. Plots of $dV/d(\ln I)$ versus I and $H(I)$ versus I obtained from the forward bias *I–V* characteristic of the Al/MV/n-Si/AuSb structure.

equation (7):

$$\frac{dV}{d(\ln I)} = \frac{nkT}{q} + IR_s, \tag{8}$$

$$H(I) = V - \left(\frac{nkT}{q}\right)\ln\left(\frac{I}{AA^*T^2}\right). \tag{9}$$

$H(I)$ is given as follows:

$$H(I) = n\Phi_b + IR_s. \tag{10}$$

A plot of $dV/d(\ln I)$ versus I will be linear and gives R_s as the slope and nkT/q as the *y*-axis intercept from equation (8). Figure 5 shows a plot of $dV/d(\ln I)$ versus I at room temperature. The values of n and R_s were calculated as $n = 4.80$ and $R_s = 3.71\,\text{k}\Omega$, respectively. It is observed that there is a relatively large difference between the value of n obtained from the forward bias ln *I–V* plot and that obtained from the $dV/d(\ln I)$–I curves. This can be attributed to the existence of the series resistance and interface states, and to the voltage drop across the interfacial layer [34].

Besides, the $H(I)$ versus I plot has to be linear according to [33]. The slope of this plot gives a different determination of R_s. Using the value of n obtained from equation (10), the value of Φ_b is obtained from the *y*-axis intercept. The $H(I)$ versus I curve is shown in figure 5. From the $H(I)$ versus I plot, Φ_b and R_s have been calculated as 0.79 eV and 3.67 kΩ, respectively.

Norde proposed an alternative method to determine the value of the series resistance. The following function has been defined in the modified Norde's method [35]:

$$F(V) = \frac{V}{\gamma} - \frac{kT}{q}\ln\left(\frac{I(V)}{AA^*T^2}\right), \tag{11}$$

where γ is an integer (dimensionless) greater than n. $I(V)$ is the current obtained from the *I–V* curve. Once the minimum of the F versus V plot is determined, the value of BH can be obtained from equation (12), where $F(V_0)$ is the minimum point of $F(V)$ and V_0 is the corresponding voltage:

$$\Phi_b = F(V_0) + \frac{V_0}{\gamma} - \frac{kT}{q}. \tag{12}$$

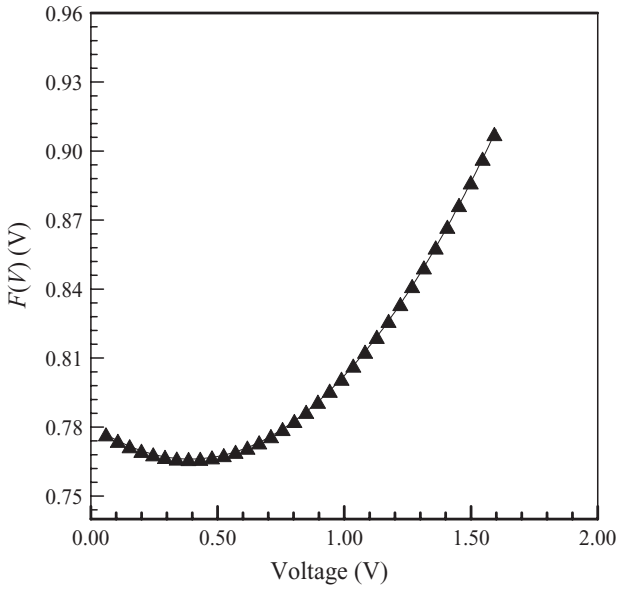

Figure 6. $F(V)$ versus V plot of the Al/MV/n-Si/AuSb structure.

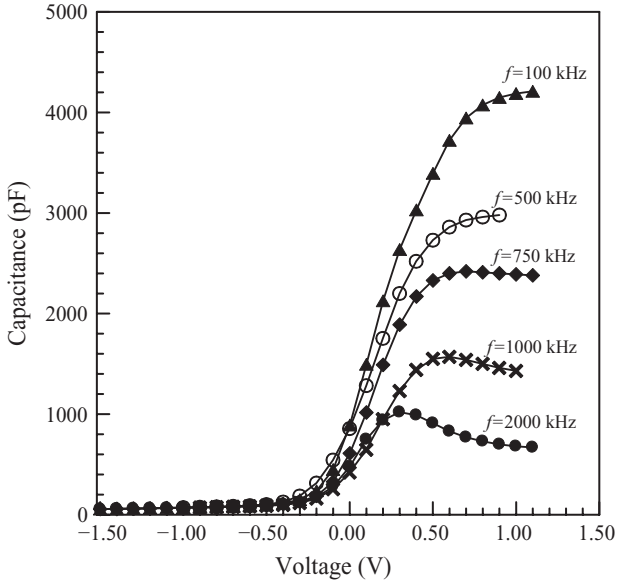

Figure 7. C–V characteristics of the Al/MV/n-Si/AuSb structure at various frequencies.

Figure 6 shows the $F(V)$–V plot of the junction. From Norde's functions, the R_s value can be determined as

$$R_s = \frac{kT(\gamma - n)}{qI}. \tag{13}$$

From the F–V plot by using $F(V_0) = 0.76$ V and $V_0 = 0.49$ V values, the values of Φ_b and R_s of the Al/MV/n-Si structure have been determined as 0.86 eV and 10.44 kΩ, respectively. There is good agreement between the values of Φ_b obtained from the forward bias ln I–V, Cheung functions and Norde functions. However, the value of the series resistance is higher than that obtained from Cheung functions. Cheung functions are only applied to the nonlinear region in the high-voltage region of the forward bias ln I–V characteristics. But, Norde's functions are applied to the full forward bias region of the ln I–V characteristics of the junctions. The value of series resistance may also be high for the higher ideality factor values. Furthermore, the value of series resistance is very high for this device. This indicates that the series resistance is a current-limiting factor for this structure. The effect of the series resistance is usually modeled with series combination of a diode and a resistance R_s. The voltage drop across a diode is expressed in terms of the total voltage drop across the diode and the resistance R_s. The very high series resistance behavior may be ascribed to the decrease of the exponentially increasing rate in current due to space-charge injection into the MV thin film at higher forward bias voltage.

C–V measurement is one of the most popular electrical measurement techniques used to characterize a Schottky diode. Generally, the capacitance measured for the Schottky diode is dependent on the reverse bias voltage and frequency. Its voltage and frequency dependence is due to the particular features of a Schottky barrier, impurity level, high series resistance, interface states and interface layer between organic layer and n-Si substrate, etc. At low frequency the capacitance measured is dominated by the depletion capacitance of the Schottky diode, which is bias dependent and frequency independent. As the frequency is increased, the total diode capacitance is affected not only by the depletion capacitance, but also by the bulk resistance and dispersion capacitance, which is frequency dependent and associated with electron emission from slowly responding deep impurity levels. Because of these effects, the capacitance dependence on bias becomes less pronounced or disappears [36].

Figure 7 shows the forward and reverse bias C–V characteristics of the structure measured for different frequencies at room temperature. For all frequencies, the capacitance remains constant in the reverse bias region. The values of the capacitance at the low frequencies (100, 500 and 750 kHz) increase in the low forward bias region until a point where it reaches a maximum value, and then is nearly constant for higher forward bias values. However, for the high-frequency values (1000 and 2000 kHz), the capacitance gradually increases to reach the maximum value with the lower forward bias and then decreases with the higher bias, which has already been observed from the pentacene-based diodes [37] and is probably related to the trapping and detrapping of the localized trap charges in the band gap of the semiconductor. The traps in the depletion region at the interface between organic and inorganic semiconductors are charged and the capacitance gradually increases when the small forward bias applied. With the higher bias the capacitance decreases due to significant carrier injection by FN tunneling and thereby the neutralization of trapped charges [37].

Figure 8 depicts the forward bias capacitance–frequency (C–f) characteristics of the Al/MV/n-Si/AuSb structure at various voltages from 0.0 to 0.40 V. It is seen from these plots that the values of the measured capacitance become almost constant up to a certain frequency value. Besides, the higher values of capacitance at low frequency are due to the excess capacitance resulting from the interface states in equilibrium with the n-Si that can follow the alternating current signal. The interface states at lower frequencies follow the alternating current signal, whereas at higher frequencies they cannot follow the alternating current signal. The values

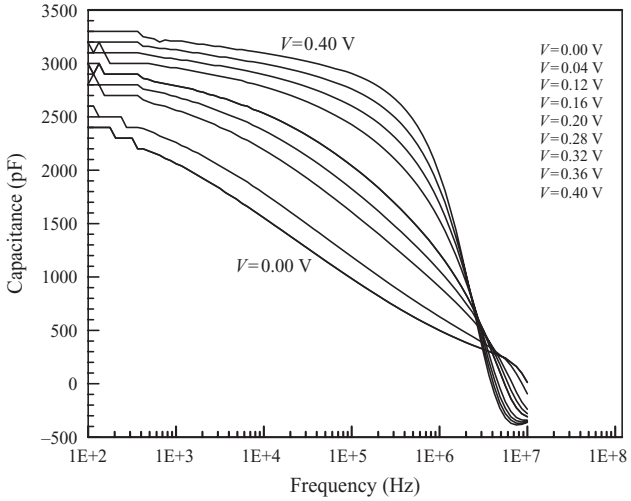

Figure 8. *C–f* characteristics of the Al/MV/n-Si/AuSb structure at various voltages.

of the capacitance at the high-frequency region originate from only space-charge capacitance. Also, in figure 8 the negative capacitance is exhibited for large frequencies. A negative capacitance phenomenon has been displayed by a variety of electronic devices, such as p–n junctions, MS Schottky diodes and GaAs/AlGaAs heterostructures. The microscopic physical mechanisms of negative capacitance in different devices are obviously different and have been ascribed mainly to contact injection, interface states or minority-carrier injection effects. The negative capacitance phenomenon could be interpreted by transient current analysis and was attributed to be a consequence of the kinetic reactivity due to the inertia (delay) of the change in the current flowing in the structure as a result of changing the applied voltage [38].

4. Conclusions

In conclusion, we have investigated the *I–V*, *C–V* and *C–f* characteristics of the Al/MV/n-Si/AuSb structure. The values of the ideality factor, series resistance and BH calculated by using different methods were compared. It was seen that there was an agreement with each other. The downward concave curvature of the forward bias *C–V* characteristics at sufficiently large voltages has been attributed to the effect of series resistance. Thus, the concavity of the forward bias *I–V* characteristics increases with increasing series resistance value. It has been seen that the values of capacitance are almost independent up to a certain value of frequency; after this value the capacitance decreases with increasing frequency. The higher values of capacitance at low frequencies have been attributed to the excess capacitance resulting from the interface states in equilibrium with the n-Si that could follow the alternating current signal.

References

[1] Prasad P N and Williams J D 1990 *Introduction to Nonlinear Optical Effects in Molecules and Polymers* (New York: Wiley)
[2] Ivanco J, Haber T, Resel R, Netzer F P and Ramsey M G 2006 *Thin Solid Films* **514** 156
[3] Jortner J and Ratner M A 1997 *Molecular Electronics* (Washington DC: American Chemical Society)
[4] Joachim C, Gimzewski J K and Aviram A 2000 *Nature* **408** 541
[5] Aydin M E, Yakuphanoglu F, Eom J H and Hwang D H 2007 *Physica* B **387** 239
[6] Gullu O, Baris O, Biber M and Turut A 2008 *Appl. Surf. Sci.* **254** 3039
[7] Campbell I H, Rubin S, Zawodzinski T A, Kress J D, Martin R L, Smith D L, Barashkov N N and Ferraris J P 1996 *Phys. Rev.* B **54** 14321
[8] Aydin M E and Yakuphanoglu F 2007 *J. Phys. Chem. Solids* **68** 1770
[9] El-Sayed S M, Hamid H M A and Radwan R M 2004 *Radiat. Phys. Chem.* **69** 339
[10] Kang M G and Park H H 2002 *Vacuum* **67** 91
[11] Nguyen V C and Kamloth K P 2000 *J. Phys. D: Appl. Phys.* **33** 2230
[12] El-Nahass M M, Abd-El-Rahman K F, Farag A A M and Darwish A A A 2005 *Org. Electron.* **6** 129
[13] Aydogan S, Saglam M and Turut A 2005 *Vacuum* **77** 269
Aydogan S, Saglam M and Turut A 2005 *Polymer* **46** 563
[14] Musa I and Eccleston W 1999 *Thin Solid Films* **343–4** 469
[15] Cakar M, Yildirim N, Karatas S, Temirci C and Turut A 2006 *J. Appl. Phys.* **100** 074505
Cakar M, Temirci C and Turut A 2004 *Synth. Met.* **142** 177
[16] Roberts A R V and Evans D A 2005 *Appl. Phys. Lett.* **86** 072105
[17] Rhoderick E H and Williams R H 1988 *Metal–Semiconductor Contacts* 2nd edn (Oxford: Clarendon)
[18] Cetinkara H A, Turut A, Zengin D M and Erel S 2003 *Appl. Surf. Sci.* **207** 190
[19] Pope M and Swenberg C E 1999 *Electronic Processes in Organic Crystals and Polymers* 2nd edn (New York: Oxford University Press) p 379
[20] Lee J, Kim S S, Kim K, Kim J H and Im S 2004 *Appl. Phys. Lett.* **84** 1701
[21] Park S Y, Lee C H, Song W J and Seoul C 2001 *Curr. Appl. Phys.* **1** 116
[22] Aydogan S, Saglam M, Turut A and Onganer Y 2005 *Synth. Met.* **150** 15
[23] Temirci C, Çakar M, Türüt A and Onganer Y 2004 *Phys. Status Solidi* a **201** 3077
[24] Kampen T U, Schuller A, Zahn D R T, Biel B, Ortega J, Perez R and Flores F 2004 *Appl. Surf. Sci.* **234** 341
[25] Bolognesi A, Di Carlo A, Lugli P, Kampen T and Zahn D R T 2003 *J. Phys.: Condens. Matter* **15** S2719
[26] Zahn D R T, Kampen T U and Mendez H 2003 *Appl. Surf. Sci.* **212–3** 423
[27] Lonergan M 2004 *Annu. Rev. Phys. Chem.* **55** 257
[28] Gullu O, Biber M and Turut A 2008 *J. Mater. Sci. Mater. Electron.* **19** 986
[29] Forrest S R 1997 *Chem. Rev.* **97** 1793
[30] Peisert H, Knupfer M and Fink J 2002 *Appl. Phys. Lett.* **81** 2400
[31] Aydogan S, Saglam M and Turut A 2008 *Microelectron. Eng.* **85** 278
[32] Turut A, Saglam M, Efeoglu H, Yalcin N, Yildirim M and Abay B 1995 *Physica* B **205** 41
[33] Cheung S K and Cheung N W 1986 *Appl. Phys. Lett.* **49** 85
[34] Kilicoglu T 2008 *Thin Solid Films* **516** 967
[35] Karatas S, Altindal S, Turut A and Cakar M 2007 *Physica* B **392** 43
[36] Aydogan S, Saglam M and Turut A 2005 *Polymer* **46** 563
[37] Lee S, Park J H and Choi J S 2003 *Opt. Mater.* **21** 433
[38] Shen W Z and Perera A G U 2001 *Appl. Phys.* A **72** 107